Continuously tunable photonic fractional Hilbert transformer using a high-contrast germanium-doped silica-on-silicon microring resonator

Hiva Shahoei,[1] Patrick Dumais,[2] and Jianping Yao[1,*]

[1]*Microwave Photonics Research Laboratory, University of Ottawa, 800 King Edward Avenue, Ontario K1N 6N5, Canada*

[2]*Communications Research Centre, 3701 Carling Avenue, Ottawa, Ontario K2H 8S, Canada*

**Corresponding author: jpyao@eecs.uottawa.ca*

Received January 28, 2014; revised March 25, 2014; accepted March 27, 2014;
posted March 28, 2014 (Doc. ID 205563); published April 30, 2014

We propose and experimentally demonstrate a continuously tunable fractional Hilbert transformer (FHT) based on a high-contrast germanium-doped silica-on-silicon (SOS) microring resonator (MRR). The propagation loss of a high-contrast germanium-doped SOS waveguide can be very small (0.02 dB/cm) while the lossless bend radius can be less than 1 mm. These characteristics lead to the fabrication of an MRR with a high *Q*-factor and a large free-spectral range (FSR), which is needed to implement a Hilbert transformer (HT). The SOS MRR is strongly polarization dependent. By changing the polarization direction of the input signal, the phase shift introduced at the center of the resonance spectrum is changed. The tunable phase shift at the resonance wavelength can be used to implement a tunable FHT. A germanium-doped SOS MRR with a high-index contrast of 3.8% is fabricated. The use of the fabricated MRR for the implementation of a tunable FHT with tunable orders at 1, 0.85, 0.95, 1.05, and 1.13 for a Gaussian pulse with the temporal full width at half-maximum of 80 ps is experimentally demonstrated.

OCIS codes: (350.4010) Microwaves; (070.0070) Fourier optics and signal processing; (130.3120) Integrated optics devices; (310.5448) Polarization, other optical properties; (060.5625) Radio frequency photonics.
http://dx.doi.org/10.1364/OL.39.002778

All-optical signal processing recently has attracted interest because of advantages such as broad bandwidth and high speed, which may not be achievable based on digital electronics. The implementation of basic signal processing blocks in the optical domain has recently been intensively investigated. One of the main signal processing blocks is a Hilbert transformer (HT) [1] including a classical HT (with an order of 1) and a fractional HT (FHT) (with a tunable order), which can be used to achieve single-sideband modulation, bandpass signal sampling, and image edge detection. A fractional HT (FHT) is a generalized form of a classical HT that provides an additional degree of freedom [2]. Different methods have been proposed to implement an HT or an FHT. Generally, an HT can be implemented based on free-space optics [2,3], fiber optics [4–10], or integrated optics [11,12]. HTs based on free-space optics usually are large and heavy and have high loss, which may not be suitable for applications where light weight and small size are required. Fiber-optics-based HTs have been extensively investigated because they have lighter weight and smaller size. In [4–7], a microwave photonic HT was implemented using a multitap microwave photonic filter. Negative taps are needed to produce a microwave photonic filter with a spectral response corresponding to an HT. In [4,5], the negative taps of the microwave photonic filter were generated by two Mach–Zehnder modulators (MZMs) biased at the quadrature points in the opposite slopes of the transfer functions. In [6], the negative taps were generated based on polarization-modulation to intensity-modulation inversion. In [7], a tunable FHT based on a nonuniformly spaced delay-line microwave photonic filter with a significantly simplified structure was proposed and demonstrated.

A sampled fiber Bragg grating (FBG) can be used to implement a classical HT [8]. An HT can also be implemented using a uniform weak-coupling FBG with a π-phase shift [9]. Recently, the inverse scattering method has been used to design and fabricate an FBG to implement a classical HT [10]. On the other hand, there also has been extensive research into the implementation of an HT based on a photonic integrated circuit (PIC). Compared to fiber-optics-based implementation, an implementation based on a PIC has significant advantages, which include a greatly reduced size, and significantly increased long-term stability. In addition, the ruggedness and low cost offered by PIC-based solutions are also expected for practical applications. In [11], a Bragg grating written in a planar silica-on-silicon (SOS) waveguide was used to implement an HT. Recently, Zhuang *et al.* proposed a tunable FHT using optical all-pass filter based on an integrated microring resonator (MRR) [12], in which the fractional order was tuned through thermally tuning the coupling coefficient and the loss factor through changing the currents sent to the two resistor-based heaters. However, this tuning mechanism needs an additional procedure in the fabrication process, and also requires additional electrical power supplies. In addition, the thermal tuning is a relatively slow procedure, with a response time between 1 and 50 ms. An all-optical approach is needed to achieve fast tuning.

In this Letter, we propose a new method to implement an FHT using a high-contrast germanium-doped SOS MRR that is optically tunable. The tunability is achieved based on the polarization dependency of the MRR by changing the polarization direction of the incident light to the MRR using a polarization controller. The polarization tuning as fast as a few microsecond can be achieved using a high-speed polarization controller. Silica is an

isotropic material; however, SOS waveguides show high polarization dependency from thermal stress. The mismatch between the thermal expansion coefficient (TEC) of the silicon substrate and the three glass layers (bottom cladding, core, and top cladding) is the main reason for this stress [13]. The induced polarization dependency has been considered a drawback in silica planar optical waveguides. Different methods have been proposed to reduce this SOS polarization dependency [14–16]. However, for the implementation of an FHT, this polarization dependency can be perfectly used to all-optically tune the coupling coefficient and the loss factor, leading to the tuning of the phase shift at the resonance wavelength, thus the fractional order of the FHT. In the implementation, the polarization direction of the input signal applied to the MRR is changed, which leads to the change of the phase shift at the resonance wavelength of the MRR, thus the fractional order is changed. A germanium-doped SOS MRR with a high index contrast of 3.8% is fabricated. The use of the fabricated MRR to implement a continuously tunable FHT is demonstrated. In the experiment, the Hilbert transformation of a Gaussian pulse with a temporal full width at half-maximum (FWHM) of 80 ps with tunable fractional orders at 0.85, 0.95, 1, 1.13, and 1.22 is realized.

An HT is an all-pass filter that shifts the phase of the negative frequency components by +90° and the phase of the positive frequency components by −90°. An FHT is a generalized HT. The frequency response of an FHT can be written as [17]:

$$H_{\mathrm{FHT}}(\omega) = \begin{cases} e^{-j\varphi}, & \omega > 0 \\ \cos(\varphi), & \omega = 0 \\ e^{+j\varphi}, & \omega < 0 \end{cases}, \tag{1}$$

where $\varphi = \rho \times \pi/2$ is the phase shift and ρ is the fractional order. As Eq. (1) shows, an FHT of an order of ρ has a magnitude response of 1 and a phase shift of $\rho\pi$ at $\omega = 0$.

The frequency response of the through port of a double-bus ring resonator can be expressed as [18]:

$$T = \alpha_c \left[\frac{t - t\alpha e^{j\theta}}{1 - \alpha t^2 e^{j\theta}} \right], \tag{2}$$

where $\theta = 2\pi n_{\mathrm{eff}} L/\lambda$ is the total round-trip phase accumulation, t is the coupling coefficient, and $\alpha = \alpha_r \cdot \alpha_c$ is the total loss factor that is the combination of the loss factor inside the ring (α_r), and the loss of the ring's coupler (α_c). The coupling coefficient and the loss factor of the MRR are strongly polarization dependent. The birefringence in an SOS waveguide originates from the thermal stress caused by the TEC mismatch of different layers during the high-temperature treatment employed in the glass deposition process of the fabrication. The thermal stress is dependent on the dopant level of the core. A higher refractive index contrast results in a higher thermal stress and correspondingly a higher polarization dependency.

By changing the polarization direction of the input pulse introduced to the ring, the resonance spectral response is changed, which leads to the change of the phase shift at the resonance wavelength. Therefore, by choosing the wavelength of the optical carrier carrying the optical pulse at the resonance wavelength, a tunable phase shift is introduced at the center of the optical pulse, and since the resonance width is ultranarrow, fractional Hilbert transformation of the pulse is obtained. The tuning of the FHT is achieved by tuning the polarization direction of the input pulse.

A high-contrast germanium-doped SOS waveguide has a low propagation loss and a low bending loss [19]. An ultralow-loss MRR with a propagation loss of 0.085 dB/cm was recorded using a germanium-doped SOS waveguide with an index contrast of 3.5% [20]. In an MRR, a lower loss would result in a higher Q factor, corresponding to a narrower resonance bandwidth. In addition, the use of a high-contrast germanium-doped SOS waveguide can reduce the minimum lossless bend radius of an MRR. A smaller radius corresponds to a larger free-spectral range (FSR). Therefore, a broadband HT can be implemented using a high-contrast MRR with a narrower resonance bandwidth and a larger FSR.

A germanium-doped waveguide with a high-refractive index core ($n_c = 1.5$) is fabricated. The wafer is oxidized to create the bottom layer. A germanium-doped layer is deposited on the top. The top cladding layer is a borophosphosilicate glass (BPSG). The core layer and the cladding layers are annealed after deposition. Since the refractive index of a pure silica is $n_b = 1.445$, a high index contrast of 3.8% is achieved ($\Delta n = (n_c - n_b)/n_b$). The cross-section of the core has a dimension of 2 μm × 2 μm. Figure 1(a) shows a schematic drawing of the waveguide cross section along with the layer compositions and thicknesses of the SOS chip. This waveguide shows a bend radius less than 1 mm [21]. A double-bus MRR with 1 mm radius of curvature and 2 μm coupler gaps is fabricated on this waveguide. This MRR shows a low propagation loss of 0.02 dB/cm. The FSR of this ring is 32 GHz, while the FWHM bandwidth of the resonance is as small as 140 MHz. The operation bandwidth of the device, which is approximately equal to two times the FSR minus the null-to-null bandwidth of the notch, is very large (0.44 nm, or 55 GHz). Therefore, this MRR is a good candidate to implement a broad bandwidth HT. An optical vector analyzer (Luna Technologies) is used to measure the transmission spectrum of the fabricated MRR. To study the polarization dependence, the polarization direction of the input light to the MRR is tuned, from the transverse electric (TE) mode to the transverse magnetic (TM) mode, by tuning a polarization controller (PC). When the polarization direction of the input light wave is oriented at a 45° angle relative to

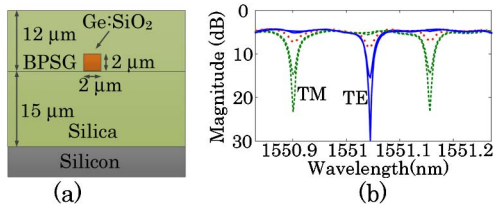

Fig. 1. (a) Schematic diagram of the waveguide cross-section and (b) transmission magnitude response of the MRR at different light polarization directions.

one principal axis of the MRR, the light wave is equally split into the TE and TM modes, shown as the transmission spectrum as a dotted red line in Fig. 1(b). If the input light wave is oriented at an angle smaller or greater than 45°, the TE mode is greater or smaller than the TM mode, shown as the solid blue line and dashed green line in Fig. 1(b). Figure 1(b) also shows that a TE mode resonance occurs at the wavelength of 1551.05 nm while a TM mode resonance occurs at 1551.15 nm due to the birefringence of the waveguide. By changing the input light wave from a TE mode to a TM mode, the depth of the TE resonance is decreased from its maximum until it vanishes and the depth of the TM mode resonance is increased to reach its maximum. Since the depth of the resonance changes when the polarization direction of the input light wave changes, the phase shift at the resonance wavelength accordingly changes (based on the Kramers–Kronig relations). This result can be used to implement a tunable FHT.

Figure 2 shows the magnitude and phase responses of the MRR around the resonance wavelength of 1551.88 nm for the input light wave at four different polarization directions. As Fig. 2 shows, by changing the polarization direction from state 1 to state 4, the depth of the resonance is increased and correspondingly the phase shift at the resonance wavelength is changed from 1.55 to 4.16 rad. In Fig. 2, the frequency responses of the MRR demonstrate that a tunable FHT can be implemented by changing the input light polarization direction. By applying a Gaussian pulse with a temporal FWHM of 40 ps centered at the resonance wavelength to the MRR, a Hilbert-transformed signal is obtained. Figure 3 shows the simulated Hilbert-transformed signals using the spectral response of the MRR for four different polarization directions that were shown in Fig. 2. The corresponding fractional orders are 0.53, 0.82, 1.14, and 1.32. For comparison, four ideally Hilbert-transformed signals with the same fractional orders are also simulated and shown in Fig. 3. As shown, the Hilbert-transformed signals using the MRR and the ideally Hilbert-transformed signals are very close. The small errors are mainly due to the notch in the magnitude response of the MRR. For an ideal FHT, the magnitude response should be constant over the bandwidth.

An experiment is then performed to evaluate the operation of the MRR as an FHT. Figure 4 shows the experimental setup. A continues wave (CW) light generated by a tunable laser source (TLS, Anritsu MG9638A) is sent to a 20-GHz MZM via a PC (PC1). A Gaussian pulse with a temporal FWHM of 80 ps is generated by a signal generator and applied to the MZM. The modulated signal at the output of the MZM is sent to an erbium-doped fiber amplifier (EDFA). A second PC (PC2), which is electronically controlled with high precision (JDS Uniphase PR2000), is used to control and tune the polarization direction of the modulated light to the MRR. Two tapered fibers are used to couple the modulated light into and out of the MRR. The optical signal at the output of the MRR is detected with a 53-GHz photodetector (PD) and the waveform is observed with a sampling oscilloscope (OSC).

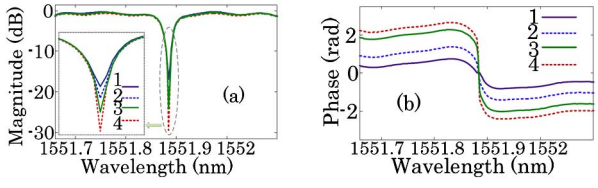

Fig. 2. (a) Transmission magnitude responses and (b) phase responses of the fabricated high-contrast SOS MRR for an input light wave with four different polarization directions.

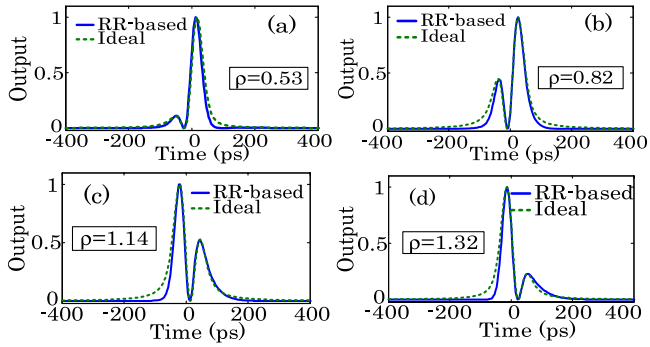

Fig. 3. Fractional Hilbert transform of a Gaussian pulse by using the spectral response of the MRR for four different polarization directions shown in Fig. 2 (solid lines). FHT orders corresponding to the polarization directions are (a) 0.53, (b) 0.82, (c) 1.14, and (d) 1.32. Fractional Hilbert transforms of an ideal Gaussian pulse with the same orders also are shown for comparison (dashed lines).

Figures 5(b)–5(f) show five fractional Hilbert-transformed signals with different fractional orders at 1, 0.85, 0.95, 1.05, and 1.13 corresponding to five different input polarization directions. Fractional Hilbert transforms of the ideal Gaussian pulse shown in Fig. 5(a) with an ideal FHT with the same orders also are simulated and shown in Figs. 5(b)–5(f) as dashed lines. As can be seen, a good agreement is reached. The root mean square (RMS) error is calculated and is less than 5%. The difference between the simulated and experimental results is mainly caused due to the nonideal Gaussian pulse and the limited bandwidth of the PD. Note that tunable magnitude response is

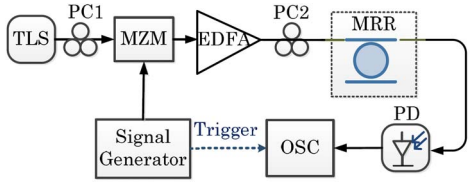

Fig. 4. Experimental setup. TLS, tunable laser source, MZM, Mach–Zehnder modulator, EDFA, erbium-doped fiber amplifier, PC, polarization controller, PD, photodetector, OSC, oscilloscope.

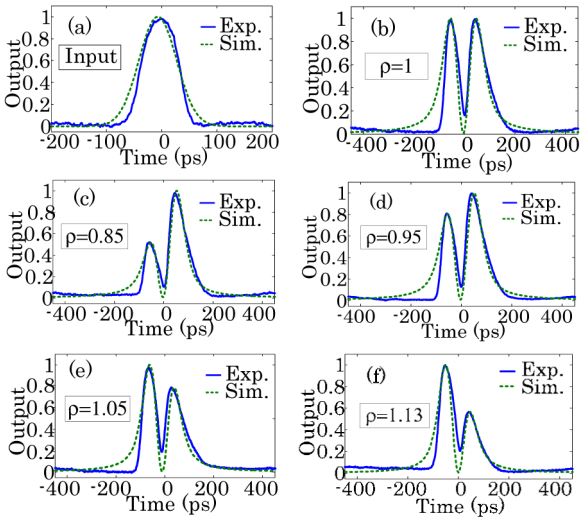

Fig. 5. (a) Experimentally generated Gaussian pulse (solid line) with a temporal FWHM of 80 ps. An ideal Gaussian pulse (dashed line) also is shown for comparison. The fractional Hilbert-transformed pulses (solid lines) with different orders of (b) 1, (c) 0.85, (d) 0.95, (e) 1.05, and (f) 1.13. Fractional Hilbert transforms of an ideal Gaussian pulse with an ideal FHT at the same orders are also shown for comparison (dashed lines).

essential to achieve a tunable HT. Since, the resonance notch is very narrow to achieve an HT, by changing the notch magnitude the power of the detected Hilbert-transformed signal is not changed significantly. In our experiment the power change is less than 8%.

In conclusion, we have proposed and experimentally demonstrated a continuously tunable FHT using a high-contrast germanium-doped SOS MRR. Two features of this MRR make it possible to operate as a tunable FHT. First, as a result of a high index contrast, the MRR has a narrow resonance and a large FSR, which is suitable for the implementation of an HT with a wide operation bandwidth. Second, the MRR is highly birefringent, by changing the polarization direction of the input light wave into the MRR, a tunable phase shift at the resonance wavelength is produced, which can be used to implement an FHT with a tunable fractional order.

A germanium-doped SOS MRR with an index contrast of 3.8% was fabricated. This fabricated MRR provides an FSR of 32 GHz and an FWHM bandwidth of the notch of 140 MHZ, which was used to implement an FHT with a wide operation bandwidth of 55 GHz. We used this fabricated MRR to experimentally demonstrate a continuously tunable FHT with tunable fractional orders at 1, 0.85, 0.95, 1.05, and 1.13, and a Gaussian pulse with a temporal FWHM of 80 ps was Hilbert-transformed at different orders.

This work was supported by the Natural Sciences and Engineering Research Council of Canada (NSERC) through its strategic grant project.

References

1. A. D. Poularikas, *Transforms and Applications Handbook*, 3rd ed. (CRC Press, 2010), Chap. 7.
2. A. W. Lohmann, D. Mendlovic, and Z. Zalevsky, Opt. Lett. **21**, 281 (1996).
3. C. S. Guo, Y. J. Han, J. B. Xu, and J. Ding, Opt. Lett. **31**, 1394 (2006).
4. H. Emami, N. Sarkhosh, L. A. Bui, and A. Mitchell, Opt. Lett. **33**, 98 (2008).
5. H. Emami, N. Sarkhosh, L. A. Bui, and A. Mitchell, Opt. Express **16**, 13707 (2008).
6. Z. Li, H. Chi, X. Zhang, and J. P. Yao, IEEE Photon. Technol. Lett. **23**, 1694 (2011).
7. Z. Li, Y. Han, H. Chi, X. Zhang, and J. P. Yao, J. Lightwave Technol. **30**, 1948 (2012).
8. X. Wang, M. Hanawa, K. Nakamura, K. Takano, and K. Nakagawa, in *Proceedings of Asia-Pacific Conference on Comunication* (2009), pp. 622–625.
9. M. H. Asghari and J. Azaña, Opt. Lett. **34**, 334 (2009).
10. M. Li and J. P. Yao, IEEE Photon. Technol. Lett. **22**, 1559 (2010).
11. C. Sima, J. C. Gates, H. L. Rogers, P. L. Mennea, C. Holmes, M. N. Zervas, and P. G. R. Smith, Opt. Lett. **38**, 727 (2013).
12. L. Zhuang, M. R. Khan, W. Beeker, A. Leinse, R. Heideman, and C. Roeloffzen, Opt. Express **20**, 26449 (2012).
13. P. Dumais, J. Lightwave Technol. **30**, 906 (2012).
14. H. H. Yaffe, C. H. Henry, R. F. Kazarinov, and M. A. Milbrodt, J. Lightwave Technol. **12**, 64 (1994).
15. A. Kilian, J. Kirchof, G. Przyrembel, and W. Wischmann, J. Lightwave Technol. **18**, 193 (2000).
16. B. M. A. Rahman, N. Somasiri, and K. T. V. Grattan, IEEE Photon. Technol. Lett. **17**, 1205 (2005).
17. H. Shahoei and J. P. Yao, IEEE Photon. Technol. Lett. **25**, 2225 (2013).
18. A. Yariv, Electron. Lett. **36**, 321 (2000).
19. A. Melloni, R. Costa, G. Cusmai, and F. Morichetti, Int. J. Mater. Prod. Technol. **34**, 421 (2009).
20. G. Bourdon, G. Alibert, A. Beguin, B. Bellman, and E. Guiot, IEEE Photon. Technol. Lett. **15**, 709 (2003).
21. P. Dumais, C. Callender, C. Blanchetiere, and C. Ledderhof, Proc. SPIE **8412**, 84120 (2012).